Microchimica Acta (2022) 189: 245
https://doi.org/10.1007/s00604-022-05352-z

ORIGINAL PAPER

# Bioconjugates of mercaptocarboxylic acids functionalized AuNP and superoxide dismutase for superoxide electrochemical monitoring

Caroline G. Sanz[1] · Daniel N. Crisan[1] · Ricardo J. B. Leote[1,2] · Melania Onea[1,2] · Madalina M. Barsan[1]

Received: 21 February 2022 / Accepted: 22 May 2022 / Published online: 8 June 2022


## Abstract

The use of gold nanoparticles/superoxide dismutase (AuNP/SOD) bioconjugates is described as building blocks in SOD biosensor development for the quantification of superoxide in cell culture media. AuNP functionalization with 11-mercaptoundecanoic acid (MUA) and 4-mercaptobenzoic acid (MBA) ($AuNP_{MUA}$ and $AuNP_{MBA}$) was used to improve SOD immobilization through EDC/NHS coupling using their –COOH terminus, leading to the formation of more stable bioconjugates. AuNP and AuNP/SOD bioconjugates were characterized by SEM to determine their size and morphology, UV–Vis for optical properties, FT-IR, and Raman spectroscopies for chemical functional group analysis and EDX for elemental analysis. Electrochemical methods were used to characterize the Au/AuNP-modified electrodes. For the optimization of the biosensor architecture, different AuNP/enzyme bioconjugates were prepared by varying the amount of both enzyme and AuNP, as well as their incubation time. Finally, the biosensors incorporating the bioconjugates were characterized by fixed potential amperometry and voltammetric analysis in order to establish the enzymatic mechanism and to elucidate the best biosensor architecture for monitoring superoxide in cell culture media. The best sensitivity value for superoxide detection corresponded to 41.2 nA μM $cm^{-2}$, achieved by a biosensor based on $AuNP_{MBA}$/SOD bioconjugates monitored through fixed potential amperometry at 0.3 V vs. Ag/AgCl, with a limit of detection of 1.0 μM, and overall very good operational stability, maintaining 91% of the initial sensitivity after 30 days. Finally, the optimized biosensor was employed for the quantification of successive additions of superoxide in cell culture media, with excellent recovery values.

**Keywords** Functionalized gold nanoparticle · Mercaptocarboxylic acid · Superoxide dismutase · Biosensor · Superoxide · Cell culture media

## Introduction

The immobilization of the enzyme is crucial in the construction of electrochemical enzyme biosensors, strategies involving the use of nanostructured materials to enhance the electronic communication between the enzymatic catalytic core and the electrode surface [1, 2]. With this aim, the use of metallic nanoparticles, with comparable dimensions to enzymes, allows the fabrication of hybrid conjugates that combine their unique electronic and catalytic properties with the specific recognition and catalytic properties of biomolecules [1]. Gold nanoparticles (AuNP) were first used as electronic bridges between redox enzymes [3], allowing direct electrical contact with the transducer, often hindered by the protein shell insulation of enzymatic active sites [4], enabling a direct electron transfer (DET) mechanism, when distances between the enzymatic redox site and the electrode surface were up to 2 nm [5]. An efficient formation of AuNP/protein conjugates is through covalent bonding, with the formation of an amide bond between native lysine or cysteine residues, the two most nucleophilic side chains on the surfaces of proteins [6], and carboxylic acid monolayers on AuNP [7, 8]. The covalent bonding is regularly established via carbodiimide cross-linker chemistry using 1-(3-dimethylaminopropyl)-3-ethylcarbodiimide hydrochloride/N-hydroxysuccinimide (EDC/NHS) [9, 10]. Furthermore, the functionalization of AuNP with -COOH groups also ensures a better dispersion of the AuNP, compared to those stabilized in citrate which tends to aggregate

✉ Madalina M. Barsan
madalina.barsan@infim.ro

[1] National Institute of Materials Physics, Str. Atomistilor 405A, 077125 Măgurele, Romania

[2] Faculty of Physics, University of Bucharest, Str. Atomistilor 405, 077125 Măgurele, Romania

at high ionic concentration and in protein solutions [11]. In this context, the synthesis of AuNP functionalized with mercaptocarboxylic acids, which bind strongly to AuNP through the thiol group, is of great interest [12], since they effectively disperse in water at neutral and basic pH levels, being highly stable in phosphate-buffer saline and cell-culture media [13]. The nature of mercaptocarboxylic acids not only influences the linkage of enzyme, in terms of quantity and conformation, but it also regulates the enzymatic reaction occurring between the enzyme redox core and the AuNP.

Reactive oxygen species, produced either from normal cell metabolisms in situ or from external sources, are able to interact with other biological species and modulate signaling pathways. However, when in excess, they confer cellular damages. Therefore, most living organisms use endogenous antioxidants, but whenever there is an imbalance, the complete removal of free radicals fails and oxidative stress can result, which can be linked to various medical conditions. Therefore, the detection of ROS has been always the focus of recent research, especially in the medical field where it goes down to in vivo detection in cellular analysis. Several biocompatible metallic nanostructured materials have been proposed for detection of $H_2O_2$ in cellular analysis [14–16]. Among ROS, superoxide high levels have been linked the most with cellular stress and oxidative damage. Fluorescence and electrochemical methods have been the commonly employed techniques for the detection of superoxide, with the electrochemical ones prevailing since they overcome the expensive costs, the long time, and non-portability of the fluorescence methods. Moreover, electrochemical biosensors based on superoxide dismutase have the advantage to selectively detect superoxide in cell culture media [17]. The main challenge associated with live/online monitoring is the nanomolar concentration of superoxide released from living cells. One way for an electrochemical sensor to achieve low detection limits is the increase of its surface area for a good dispersion of the biosensing element, which is usually done by employing nanostructured materials. Another challenge is the biocompatibility of the nanomaterial with the biological molecules, especially in biomedical applications [18]. Therefore, the aim of the present study is to develop and characterize novel SOD biosensors based on building blocks of highly biocompatible AuNP with SOD (AuNP/SOD) bioconjugates. Two mercaptocarboxylic acids were investigated, one aliphatic, 1-mercaptoundecanoic acid (MUA), which is commonly used [19, 20] and one aromatic, the 4-mercaptobenzoic acid (MBA), that, from our knowledge, was not investigated for enzyme immobilization. Even though aromatic ligands have less conformational flexibility than aliphatic ligands [12], they can effectively bind proteins and maintain a good electron transfer. The main goal is to establish how the ligand nature of AuNP influences their dispersion and electronic properties [21] which will have a great impact on the enzyme immobilization and electron transfer processes within the AuNP/SOD-based biosensor.

For this, citrate stabilized AuNP ($AuNP_{CIT}$) and AuNP functionalized with MUA and MBA ($AuNP_{MUA}$ and $AuNP_{MBA}$) were synthesized and characterized by scanning electron microscopy (SEM) to determine size and morphology, UV–Vis spectroscopy for optical properties, transmission FT-IR, and Raman spectroscopies for chemical functional group analysis and energy dispersive X-ray microanalysis (EDX) for elemental analysis. Cyclic voltammetry (CV) and electrochemical impedance spectroscopy (EIS) enabled the characterization of AuNP modified electrodes, in terms of electroactive areas and electron transfer coefficients. Different AuNP/SOD bioconjugates were prepared using the EDC/NHS linkage, by varying the amount of both enzyme and AuNP, as well as their incubation time. The biosensors based on the obtained bioconjugates were characterized by fixed potential amperometry (CA) and voltammetric analysis in order to establish the enzymatic mechanism and to choose the best biosensor architecture for monitoring superoxide in cell culture media.

## Experimental

### Reagents

Superoxide dismutase from bovine erythrocytes (SOD), potassium superoxide ($KO_2$), acetic acid (HA), 1-ethyl-3-(-3-dimethylaminopropyl) carbodiimide hydrochloride (EDC), N-hydroxysuccinimide (NHS), sodium phosphate monobasic ($NaH_2PO_4$), sodium phosphate dibasic ($Na_2HPO_4$), ethanol (EtOH), dimethylformamide (DMF), and dimethyl sulfoxide (DMSO) were from Sigma-Aldrich. For the AuNP synthesis and functionalization, chloroauric acid trihydrate, 11-mercaptoundecanoic acid (MUA), 4-mercaptobenzoic acid (MBA), and citrate salt, from Sigma-Aldrich, were used. Phosphate buffer (PB) 0.1 M, pH 8.0, was prepared by dissolving the appropriate amount of $Na_2HPO_4$ and $NaH_2PO_4$ in deionized water. Stock solutions of $KO_2$ were prepared in DMSO. 4% w/v EDC was prepared in ethanol and 1% w/v NHS was prepared in water. SOD was dispersed in 0.1 M PB, pH 8.0, and stored in − 20 °C when not in use. DMEM (Dulbecco's Modified Eagle Medium), from Thermo Fisher Scientific, was used as cell culture media and contained amino acids, inorganic salts, vitamins, and glucose.

All buffer solutions were prepared using Millipore Direct-Q ultrapure water with resistivity ≥ 18 MΩ cm.

### Instrumentation

All electrochemical measurements were conducted on a three-electrode system comprising a gold electrode (1.6 mm diameter, 0.02 $cm^2$), a platinum wire, and Ag/AgCl

(saturated KCl) as working, auxiliary, and reference electrodes, respectively, in an electrochemical cell containing 2-mL electrolyte, on a MultiAutolab M101 potentiostat/galvanostat running NOVA 2.1.4 software (Metrohm Autolab, Utrecht, The Netherlands).

FT-IR was carried out on a Jasco FT/IR-6800 Spectrometer in transmittance mode. Raman Sspectra were recorded on a Horiba Scientific LabRAM HR Evolution Raman spectrometer equipped with a Kimmon IK Series He-Cd Laser source with an excitation wavelength of 633 nm (4000–50 $cm^{-1}$ wavelength interval, 5-s acquisition time, and 20 accumulations). SEM and EDX of here synthesized AuNP, as well as the AuNP/SOD bioconjugates, were carried out at a Gemini 500 XVP at different magnifications. Ultraviolet–visible (UV–vis) spectra were recorded on a Varian Cary 5000 UV–Vis-NIR Spectrophotometer.

The pH measurements were done on a Hanna HI 9124 N portable pH meter.

All experiments were carried out at room temperature (25 ± 1 °C).

### Electrode surface cleaning procedure

The bare gold electrode was initially cleaned by mechanical polishing using a 3-µm particle size diamond spray at a polishing pad, followed by recording CVs in 0.05 M $H_2SO_4$ between − 0.2 and 1.4 V at 100 mV $s^{-1}$. The electrode was thoroughly rinsed with water and isopropyl alcohol and dried under a $N_2$ flux before the biosensor constructions.

### AuNP synthesis

Citrate stabilized gold nanoparticles ($AuNP_{CIT}$) were synthesized using the Turkevich method [22]. 11-Mercaptoundecanoic acid AuNP ($AuNP_{MUA}$) and 4-mercaptobenzoic acid AuNP ($AuNP_{MBA}$) were synthesized from $AuNP_{CIT}$ by ligand exchange according to protocols described in the literature [23] (see detailed description in ESM S1).

### Au/AuNP/SOD biosensor construction

Two biosensor constructions were based on (i) the use of bioconjugates prepared in situ directly at the electrode surface to get Au/$AuNP_{CIT}$/SOD, Au/$AuNP_{MUA}$/SOD, and Au/$AuNP_{MBA}$/SOD, with final SOD concentration of 0.25, 0.50, and 1.00 mg $cm^{-2}$, and for AuNP, 0.10, 0.15, and 0.20 mg $cm^{-2}$, respectively, and (ii) pre-made bioconjugates in the volume ratio 3:1:0.5 AuNP/SOD/NHS incubated for 1 day in a thermomixer at 25 °C and 400 rpm. In all cases, the cross-linking agent NHS was of 4% w/v and EDC of 1% w/v (for further information, see ESM S1). All biosensors were left to dry for at least 2 h and stored in 0.1 M PB, pH 8.0, at 4 °C when not in use.

## Results and discussion

### Characterization of AuNP and AuNP/SOD bioconjugates

#### Transmission FT-IR, Raman, and energy-dispersive X-ray spectroscopy

AuNP were characterized initially by Transmission FT-IR (see S2 for detailed discussions and Fig. S1) and Raman spectroscopies for chemical functional group analysis, both showing differences between the AuNP alone and when present in the AuNP/SOD bioconjugates. The Raman spectra of $AuNP_{MUA}$ and $AuNP_{MBA}$, Fig. S2, showed vibrations consistent with peak patterns reported in the literature for MUA [24] and MBA, respectively [25].

EDX elemental analysis showed for all AuNP/SOD bioconjugates abundant regions of sulfur and phosphorus overlapping the gold regions (see S3 for detailed information and Fig. S3).

#### Scanning electron microscopy and UV–Vis spectroscopy

SEM images recorded at the three different AuNP and the corresponding AuNP/SOD bioconjugates are displayed in Fig. 1. SEM analysis revealed a size of 19.0 ± 4.6 nm for $AuNP_{CIT}$ and a disperse morphology (see Table S1). The functionalization with MUA and MBA does not affect the size of AuNP; however, it is observed that $AuNP_{MUA}$ tends to form aggregates as mono-layered populations (Fig. 1B1), while $AuNP_{MBA}$ aggregate into multilayered structures (Fig. 1C1). The immobilization of SOD on the AuNP did not have a significant influence on neither the size nor the dispersion of the AuNP in the corresponding bioconjugates architectures (Fig. 1A2–C2). The clarity of the AuNP in SEM was diminished due to the shrouding effect the enzyme molecules produce. $AuNP_{CIT}$ were generally dispersed in the SOD cloud, while $AuNP_{MBA}$ and $AuNP_{MUA}$ were clustered and surrounded by SOD.

In correlation with the observed sizes and morphologies observed by SEM, the UV–Vis measurements (inset of Fig. 1A1–C1) showed the expected absorbance and red color for $AuNP_{CIT}$ of this size, while $AuNP_{MUA}$ were blue/purple due to aggregation and the nanoparticle ligands [26]. $AuNP_{MBA}$ had no distinctive color and presented a broad absorbance spectrum with no particular maxima. This was attributed to the loss of the localized surface plasmon resonance as a consequence of the multilayered aggregated structures [21]. Immobilization of SOD did not affect the size of the nanoparticles in all cases.

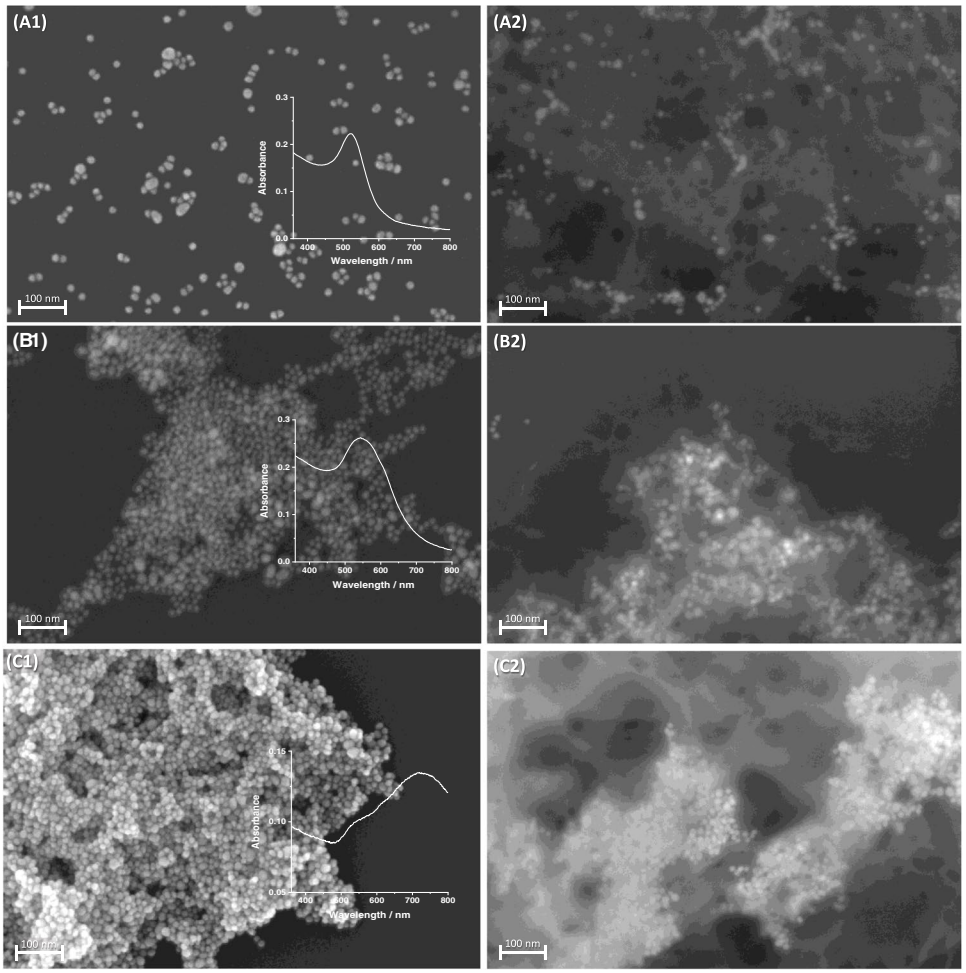


**Fig. 1** SEM Images of AuNP functionalized with **A1** citrate ($AuNP_{CIT}$), **B1** MUA ($AuNP_{MUA}$), and **C1** MBA ($AuNP_{MBA}$). SEM images of **A2** $AuNP_{CIT}$/SOD, **B2** $AuNP_{MUA}$/SOD, and **C2** $AuNP_{MBA}$/SOD bioconjugates. Inset corresponds to the UV–vis spectra of the respective functionalized AuNP

## Cyclic voltammetry and electrochemical impedance spectroscopy of Au/AuNP-modified electrodes

The electrochemical properties of Au/AuNP-modified electrodes were evaluated by CV, Fig. S4A. As a result of the increase in surface electroactivity upon AuNP immobilization, the electroactive area values for $Au/AuNP_{CIT}$ and $Au/AuNP_{MBA}$ with 90% and 30% higher compared to the unmodified Au electrode. There was no voltammetric response of the redox probe at the $Au/AuNP_{MUA}$-modified electrode, most likely due to the presence of a nonconductive aliphatic side chain that blocks the electron transfer process. The values of charge transfer coefficients $\alpha$ were calculated to be 0.70 and 0.72, and the charge transfer rate constants, $k_0$ (Nicholson method), were $2.4 \times 10^{-1}$ cm $s^{-1}$ and $2.2 \times 10^{-1}$ cm $s^{-1}$ for $Au/AuNP_{CIT}$ and $Au/AuNP_{MBA}$, respectively. The results indicate an increase in the charge transfer kinetics at both constructions compared to that observed at bare gold electrodes ($\approx 3 \times 10^{-2}$ cm $s^{-1}$).

The Au/AuNP-modified electrodes were characterized also by EIS at open circuit potential (OCP), Fig. S4B. $R_\Omega$ represents the ohmic drop and resistance caused by the electrical contacts with a constant value of ≈10 Ω. The first $R_1CPE_1$ represents the Au/AuNP interface, and the second $R_2CPE_2$ corresponds to the electrode/electrolyte interface. The results obtained by fitting the spectra are shown in Table S2. The $CPE_1$ values reflect the charge storage capacity generated by the coverage and/or distribution of AuNP at the Au electrode surface. AuNP functionalized with different ligands leads to different coverage degrees and different aggregate dimensions (seen in SEM images), with a great influence on Au/AuNP electroactivities. Therefore, the values of $CPE_1$ decreases in the following order: $Au/AuNP_{CIT} > Au/AuNP_{MBA} > Au/AuNP_{MUA}$, in agreement with the CV and SEM. Inversely, $R_1$ increase in the order $Au/AuNP_{CIT} < Au/AuNP_{MBA} < Au/AuNP_{MUA}$ and is highest in the case of $AuNP_{MUA}$ due to the charge transfer hindrance from the alkyl chain barrier at the AuNP surface.

The values calculated for $R_2/CPE_2$ also reflect the diminished charge storage capacity of AuNP with the MUA functionalization and the limitation of charge transfer is visible by the large $R_2$ values of the $Au/AuNP_{MUA}$.

It was observed that $\alpha_2$ values, which reflect the morphology of the Au/AuNP at the solid/liquid interface, increase from 0.88 to 0.93 and 0.98 for $AuNP_{CIT}$, $AuNP_{MBA}$, and $AuNP_{MUA}$, respectively, reflecting the formation of uniform and nonporous layers of $AuNP_{MUA}$ at the surface of Au electrodes, in agreement with the morphological studies in Sections "Transmission FT-IR, Raman and energy-dispersive X-ray spectroscopy" and "Scanning electron microscopy and UV-Vis spectroscopy".

### Cyclic and square wave voltammetry of Au/AuNP/SOD biosensors

CV was recorded at Au/$AuNP_{CIT}$/SOD, Au/$AuNP_{MUA}$/SOD, and Au/$AuNP_{MBA}$/SOD biosensors (see Fig. 2 for 0.50-mg $cm^{-2}$ SOD containing biosensors). Increasing amounts of enzyme of 0.25-, 0.50-, and 1.00-mg $cm^{-2}$ SOD were tested, and it was observed that the capacitive currents decrease with the increase in enzyme amount, consistent with the adsorption of organic films with low dielectric constants on the surface of the electrode [27] (see Figs. S5 and S4 in ESM for detailed discussion).

## Optimization of Au/AuNP/SOD biosensor construction by fixed potential amperometry

Bioconjugate formation and stability are highly affected by the incubation procedure of the two components. Different methodologies for biosensor construction were evaluated: (i) the bioconjugate formation in situ, through drop casting of both AuNP and SOD simultaneously on the electrode surface, in the presence of EDC/NHS and (ii) the use of pre-made bioconjugates which involved the incubation of both components for 1 day prior to electrode modification; moreover, to achieve optimal anchoring of the enzyme, NHS was also added alongside AuNP and SOD, with EDC being finally added when drop casting the electrode.

### Simultaneous drop casting of AuNP with SOD

**Effect of applied potential** The operational potential was initially optimized for the Au/$AuNP_{CIT}$/SOD biosensor by recording the amperometric response of 25 μM superoxide at 0.0, 0.1, 0.2, 0.3, and 0.4 V vs. Ag/AgCl. An increase in sensitivity values was observed for higher applied potential values, similar to those previously observed at similar biosensors [17]. Still, in order to avoid possible interference effect, 0.3 V vs. Ag/AgCl was chosen for further CA measurements.

**Effect of AuNP type** The CA response at 0.3 V vs. Ag/AgCl for Au/$AuNP_{CIT}$/SOD, Au/$AuNP_{MUA}$/SOD, and Au/$AuNP_{MBA}$/SOD biosensors (Fig. 3A) revealed higher sensitivity values for the Au/$AuNP_{CIT}$/SOD biosensor (47.7 nA μM $cm^{-2}$), in agreement with highest electroactive areas and a faster electron transfer rate coefficient. For Au/$AuNP_{MUA}$/SOD and Au/$AuNP_{MBA}$/SOD biosensors, the side chain of mercaptocarboxylic acids interfere with the charge transfer between the AuNP and the enzyme, resulting in lower sensitivity values (21.2 and 24.5 nA μM $cm^{-2}$, for Au/$AuNP_{MUA}$/SOD and Au/$AuNP_{MBA}$/SOD) (Fig. 3B).

The repeatability of SOD biosensors was assessed by performing subsequent CA measurements at the same biosensor for 5 injections of 5-μM superoxide ($n = 3$) and revealed a higher variation in the sensitivity values for the $AuNP_{CIT}$/SOD-based biosensor. Moreover, reproducibility studies performed at three different biosensors of each type indicated that the use of $AuNP_{CIT}$ leads to less reproducible biosensor architectures, with RSD value of 9.0%, higher when compared to 5.5 and 6.0% for $AuNP_{MUA}$ and $AuNP_{MBA}$, respectively. These can be attributed to the nature of AuNP/SOD bioconjugates, the enzyme being only electrostatically immobilized at $AuNP_{CIT}$, compared to a more stable covalent immobilization in the case of $AuNP_{MUA}$ and $AuNP_{MBA}$

The operational stability in time of all SOD biosensors was assessed during a period of 21 days, Fig. 3C, where the higher loss of sensitivity is observed for Au/$AuNP_{CIT}$/SOD,

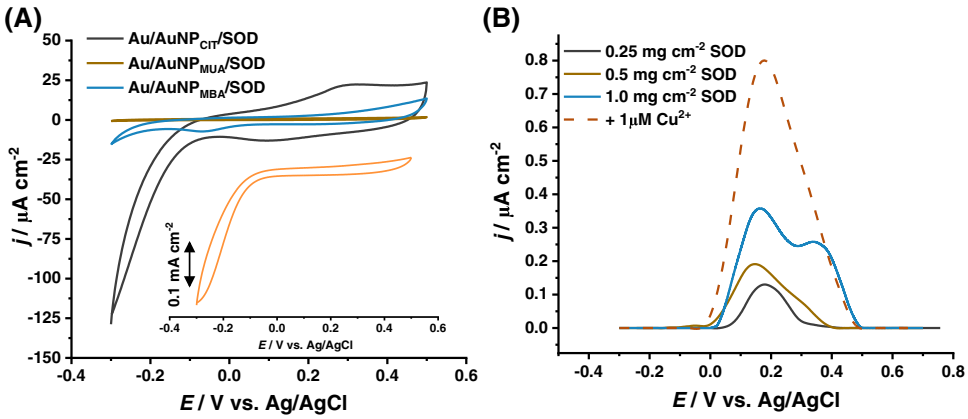


**Fig. 2** **A** CVs in 0.1 M PB, pH, 8.0, obtained at the Au/AuNP/SOD biosensors for 0.50-mg $cm^{-2}$ SOD and **B** SWV at Au/$AuNP_{MUA}$/SOD biosensor for 0.25, 0.50, and 1.00-mg $cm^{-2}$ SOD, with the addition of 1 μM $Cu^{2+}$

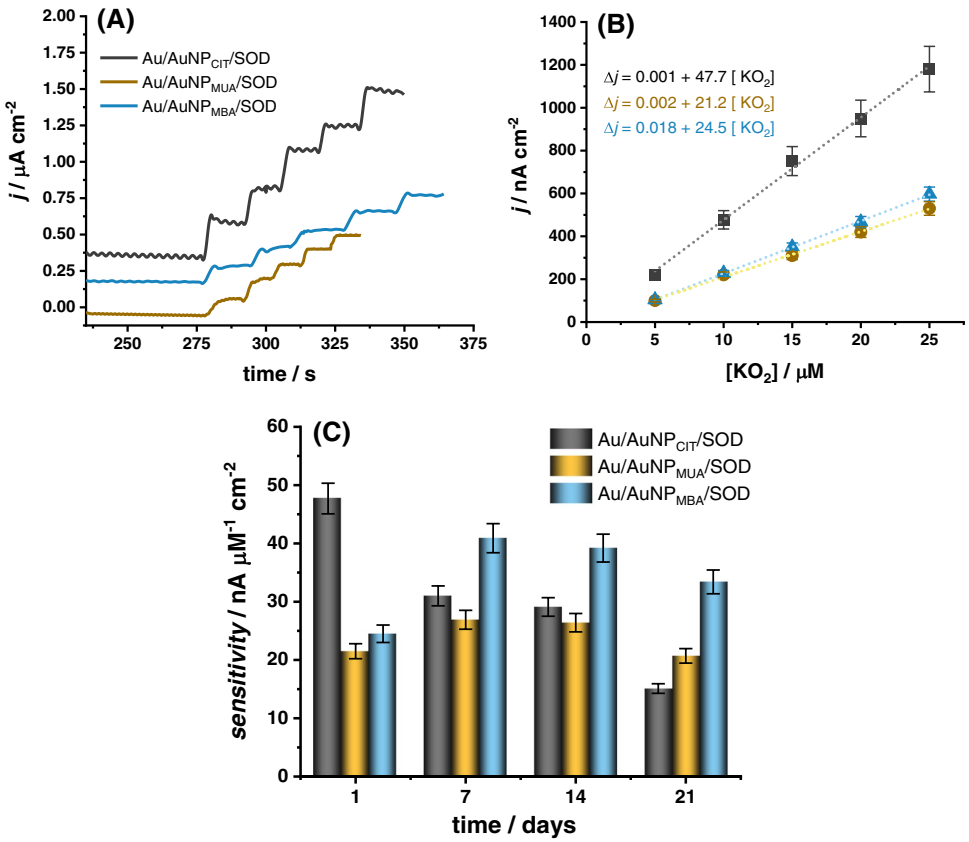


**Fig. 3** **A** Fixed potential amperometric response at Au/AuNP/SOD biosensors at 0.3 V vs. Ag/AgCl in 0.1 M PB, pH, 8.0, upon successive additions of 5 µM $KO_2$, **B** corresponding calibration plots based on amperometric data, and **C** evolution of sensitivity values of each biosensor construction during a period of 21 days

retaining only 31.6% of its initial sensitivity after 21 days. The lower stability of Au/AuNP$_{CIT}$/SOD biosensor can be attributed to a higher degree of enzyme leaching to the solution over time due to the weaker interaction within the AuNP$_{CIT}$/SOD bioconjugate.

The sensitivity values of Au/AuNP$_{MUA}$/SOD and Au/AuNP$_{MBA}$/SOD biosensors, however, increased during the first 14 days. It notes that there was a substantial increase after the first day of storage (data not shown), attributed to a rearrangement of the enzyme to a configuration that ensures a higher degree of AuNP electronic communication with the enzymatic redox core.

After 21 days of storage, the higher sensitivity values were observed for Au/AuNP$_{MBA}$/SOD, attributed to (i) a higher enzyme load within the multi-layered structure of AuNP$_{MBA}$/SOD bioconjugates, clearly observed in SEM images: (ii) better electronic conductivity due to the delocalized π-electrons of the aromatic ring which increases the electrical conductivity through the bioconjugate, in agreement with CV measurements in Sections "Cyclic voltammetry and electrochemical impedance spectroscopy of Au/AuNP-modified electrodes" and "Cyclic and square wave voltammetry of Au/AuNP/SOD biosensors"; and (iii) a higher degree of AuNP surface available for the electron transfer.

Control measurements were conducted for biosensor constructions lacking the cross-linking agents (data not shown) and revealed significantly lower sensitivities and stability for all three biosensors.

To conclude, the stability of the three types of biosensors underlines the importance of the AuNP functionalization with mercaptocarboxylic acids, for an effective enzyme immobilization via EDC/NHS coupling, thus ensuring a higher amount of enzyme retained in time at the surface of the electrode.

**Effect of AuNP and enzyme load** CA at 0.3 V vs. Ag/AgCl recorded at different Au/AuNP/SOD biosensor constructions after one day of storage, containing different AuNP and enzyme amounts, was tested in order to optimize biosensor architecture. The change in biosensor sensitivity with AuNP concentration is depicted in Fig. 4A (for 0.10-, 0.15-, and 0.20-mg cm$^{-2}$ AuNP) and with enzyme concentration in Fig. 4B (for 0.25-, 0.50-, and 1.00-mg cm$^{-2}$ SOD).

It was observed that the sensitivity response of Au/AuNP/SOD biosensors constructed using 0.10-mg cm$^{-2}$ AuNP is the lowest, probably due to an insufficient amount of nanoparticles able to anchor the amount of enzyme employed (0.50-mg cm$^{-2}$ SOD) and/or to enable an efficient electronic conductivity due to a higher degree of proteic build-up. In the case of Au/AuNP$_{CIT}$/SOD, higher sensitivity values were

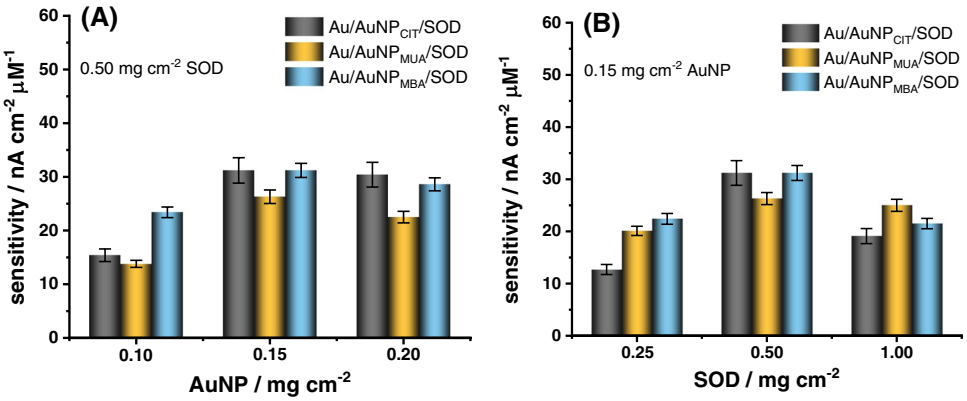


**Fig. 4** Influence of the amount of (**A**) AuNP (0.5-mg $cm^{-2}$ SOD) and (**B**) SOD enzyme (0.15-mg $cm.^{-2}$ AuNP) on sensitivity values of Au/AuNP/SOD biosensors for superoxide detection (0.3 V vs. Ag/AgCl, 0.1 M PB, pH 8.0)

obtained employing 0.15-mg $cm^{-2}$ AuNP. The sensitivity values Au/$AuNP_{MUA}$/SOD and Au/$AuNP_{MBA}$/SOD biosensors containing 0.20-mg $cm^{-2}$ AuNP were only slightly higher when compared to 0.15-mg $cm^{-2}$ AuNP containing ones, in which difficulties in charge transfer for 0.20-mg $cm^{-2}$ AuNP constructions might be related to a higher degree of AuNP aggregation.

The sensitivity variation of Au/$AuNP_{CIT}$/SOD biosensors with the enzyme concentrations (Fig. 4B) indicated the highest sensitivity for 0.50-mg $cm^{-2}$ SOD. Therefore, the best configuration for Au/AuNP/SOD biosensors was chosen to be that of 0.15-mg $cm^{-2}$ AuNP and 0.50-mg $cm^{-2}$ SOD.

### Drop-casting of incubated AuNP/SOD bioconjugates

SOD biosensors were also constructed using a pre-made bioconjugate solution (AuNP/$SOD_{INC}$), prepared by incubating for 1-day AuNP and SOD together, as described in Section "Au/AuNP/SOD biosensors construction". The obtained biosensors, Au/$AuNP_{CIT}$/$SOD_{INC}$, Au/$AuNP_{MUA}$/$SOD_{INC}$, and Au/$AuNP_{MBA}$/$SOD_{INC}$, were evaluated using the same experimental conditions and CA responses at 0.3 V vs. Ag/AgCl with the corresponding calibration curves are shown in Fig. 5.

The biosensor's responses containing the pre-made bioconjugates were compared to those obtained with the simultaneous drop casting of AuNP and SOD for the bioconjugates formation in situ (Section "Simultaneous drop casting of AuNP with SOD"). The amperometric signal stability is slightly affected for higher concentration values of superoxide, being a direct result of the competition between the chemical dismutation of superoxide in water (a second-order kinetic reaction) and the enzyme-catalyzed reaction. Firstly, a wider linear range was achieved for all biosensor constructions and higher sensitivities for the ones containing $AuNP_{MUA}$ and $AuNP_{MBA}$. The Au/$AuNP_{CIT}$/$SOD_{INC}$ biosensor presented lower sensitivity values than observed for Au/$AuNP_{CIT}$/SOD, due to the lack of stabilization of the AuNP in the presence of SOD over time. On the contrary, for Au/$AuNP_{MUA}$/$SOD_{INC}$ and Au/$AuNP_{MBA}$/$SOD_{INC}$ biosensors, an increase in sensitivity values was obtained, being highest for Au/$AuNP_{MBA}$/$SOD_{INC}$. The limits of detection were calculated based on 3**SD*/slope, for which the Au/$AuNP_{MBA}$/$SOD_{INC}$ presented the lowest values of 1.0 µM. The theoretical LD corresponded to the real detection limit, found to be 1.2 µM – the lowest concentration that leads to an increase in current three times higher than the value of the background noise.

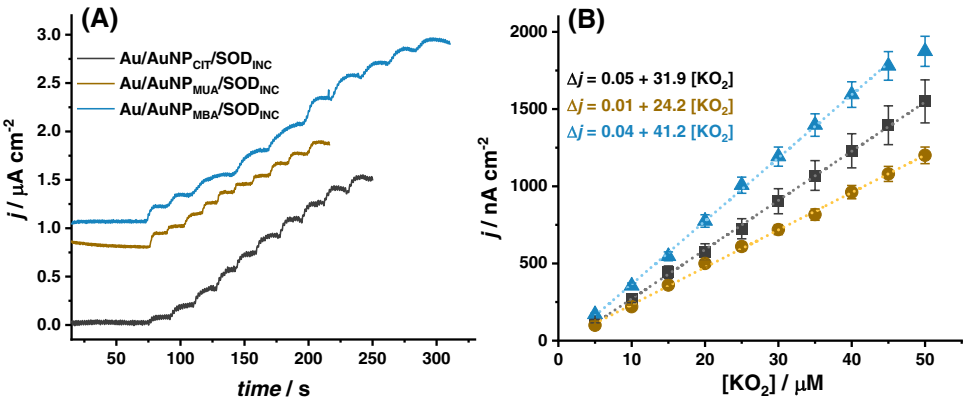


**Fig. 5** **A** Fixed potential amperometric response at Au/AuNP/$SOD_{INC}$ biosensors at 0.3 V vs. Ag/AgCl in 0.1 M PB, pH 8.0, upon successive additions of 5 µM $KO_2$ and **B** corresponding calibration plots based on amperometric data

Au/AuNP$_{MBA}$/SOD$_{INC}$ biosensor was subjected to further investigations as follows. Repeatability studies at Au/AuNP$_{MBA}$/SOD$_{INC}$ were assessed by performing subsequent measurements ($n = 3$) at the same Au/AuNP$_{MBA}$/SOD$_{INC}$ biosensor, with less than 3% variation between the sensitivity values obtained. The RSD for 3 different biosensors was only 3.8%. Long-term stability was assessed after 30 days (with 3 calibration curves being recorded each week), the biosensor retaining 91.0% of its initial response.

All the above results illustrate the increased performance of the Au/AuNP$_{MBA}$/SOD$_{INC}$ when compared to the Au/AuNP$_{MBA}$/SOD biosensor, being therefore chosen for superoxide detection in cell culture media.

## Superoxide determination in cellculture media at Au/AuNP$_{MBA}$/SODINCbiosensor

Several applications of gold nanoparticles are described within living cell assays, where their biocompatibility and ability to act as probes, anchor surfaces [4], and signal amplifiers [28] are often exploited. In this context, we describe the use of Au/AuNP$_{MBA}$/SOD$_{INC}$ for applications in superoxide monitoring in cell culture media.

The influence of common electroactive interferents on the biosensor performance was monitored by fixed potential amperometry at 0.3 V vs. Ag/AgCl in 0.1 PB pH 8.0. For this, successive additions of 5 µM of $H_2O_2$, uric acid (UA), dopamine (DA), and ascorbic acid (AA) were conducted in between additions of 5 µM of $KO_2$. A small increase in current was observed for DA and UA (10% of the response to superoxide), illustrating the increased selectivity of the proposed biosensor for superoxide monitoring. The $H_2O_2$ can be also monitored electrochemically in cell cultures, but its response appears at higher overvoltage, as shown in [29].

For the detection of superoxide in unknown samples with the here developed biosensor, the buffer solution to be employed must be in the pH range between 6 and 8, with the injection of the probe in a lower concentration range (if possible) prior to the addition of known concentrations of superoxide (5 µM $KO_2$). This may require the dilution of the sample, which brings advantages since the matrix effect is minimized.

The envisioned applicability of the Au/AuNP$_{MBA}$/SOD$_{INC}$ biosensor is the in situ detection of superoxide released from cells in close proximity to the biosensor surface, in cell culture media under external stimuli. Therefore, the performance of the biosensor was evaluated by fixed potential amperometry at 0.3 V vs. Ag/AgCl in DMEM cell culture media (with high glucose content amongst other vitamins and nutrients), which has an initial superoxide concentration of zero. The results were compared to that obtained at the same biosensor in 0.1 M PB pH 8.0, Fig. S6. A similar sensitivity value was obtained in DMEM, being 40.5 compared to 41.2 µA µM$^{-1}$ cm$^{-2}$ in buffer solutions with very high recovery values, Table 1.

The interference study together with the recovery study results which revealed RSD values of less than 5% for the biosensor in DMEM supports the applicability of such biosensors for the in vivo monitoring of superoxide released from stressed damaged cells.

## Comparison with other AuNP-based sensors and biosensors

Different AuNP-based biosensors have been described in literature, where the use of different methodologies for enzyme immobilization, as well as the influence of nanoparticle functionalization has been exploited to achieve direct electron transfer between the active site and the transducer surface, Table 2. The enzymatic mechanism is directly dependent on the biochemical reaction of interest in regards to the enzymatic active site. It is clear that for enzymes that contain metallic centers, such as laccase, SOD, cytochrome C, and horseradish peroxidase, the operational potential is slightly positive, with the signal from the oxidation of the metallic center being directly measured following the enzymatic reaction, often through fixed potential amperometry or pulsed voltammetric techniques. The analytical parameters obtained at the Au/AuNP$_{MBA}$/SOD$_{INC}$ biosensor for superoxide monitoring are similar to other enzymatic biosensors based on functionalized AuNP, which illustrates the versatility of AuNP for third generation biosensor construction, with increased sensitivity values and selectivity even when compared to non-enzymatic ensembles.

Enzyme-less AuNP-based sensor for the detection of superoxide have also been reported, based on dendrimer stabilized AuNP [37] and on hybrids containing other nanostructured and redox mediator materials, such as conducting polymers together with $Fe(CN)_6]^{4-}$ and carbon nanotubes [38], as well as hemin and electrochemically reduced graphene [39]. They mostly have low operating stability and require a higher overvoltage, lacking also the selectivity conferred by SOD.

**Table 1** Recovery studies for superoxide quantification at Au/AuNP$_{MBA}$/SOD$_{INC}$ biosensor in the cell culture media (DMEM) at 0.3 V vs. Ag/AgCl ($n = 3$)

| Added/µM | Found/µM | RSD/% | Recovery/% |
|---|---|---|---|
| 0.00 | 0.00 | 0.0 | 100 |
| 5.00 | 6.50 | 7.0 | 129 |
| 10.0 | 11.5 | 5.0 | 114 |
| 15.0 | 15.9 | 5.8 | 106 |
| 20.0 | 20.4 | 6.4 | 101 |
| 25.0 | 23.7 | 4.9 | 94.9 |

**Table 2** Enzymatic biosensors based on functionalized AuNP DET

| AuNP functionalization | Enzyme | Technique | Sensitivity/ $\mu A\ \mu M^{-1}\ cm^{-2}$ | LoD/ μM | Ref |
|---|---|---|---|---|---|
| Citrate | HRP | CA at 0.3 V | 220 | 14 | [30] |
| | GOx | DPV | 5.1 | 5.9 | [31] |
| PEI | Laccase | SWV | $1.6e^3$ | 0.16 | [32] |
| Cysteine | SOD | CA at -0.15 V | 0.022 | 0.1 μM | [33] |
| Cysteine | SOD | CA at 0.3 V | 0.05 – 440 μM | unspecified | [34] |
| MUA | ChOx | CV | 45 | 34.6 | [35] |
| MPA | Cyt C | CA at 0.15 V | - | 50 ng $mL^{-1}$ | [36] |
| MBA | SOD | CA at 0.3 V | 41.2 | 1.0 | This work |

CA, fixed potential amperometry; PEI, polyethyleneimine; MUA, mercaptoundecanoic acid; MPA, mercaptopropionic acid; MBA, 4-mercaptobenzoic acid; HRP, horseradish peroxidase; GOx, glucose oxidase; OxOx, oxalate oxidase; ChOx, cholesterol oxidase

## Conclusions

The effect of AuNP stabilized in citrate ($AuNP_{CIT}$) and functionalized with mercaptocarboxylic acids ($AuNP_{MUA}$ and $AuNP_{MBA}$) in the immobilization of superoxide dismutase and biosensor performance was evaluated. AuNP and AuNP/SOD bioconjugates presented differences in the FT-IR and Raman spectra, while the EDX analysis also revealed the presence of the enzyme in bioconjugates. SEM images showed that AuNP retained their nanometric size upon functionalization, with their distribution differing from mono-layered to multilayered aggregates for $AuNP_{MUA}$ and $AuNP_{MBA}$, respectively. The electrochemical properties of Au/AuNP modified electrodes showed an increase in both electroactive areas and charge transfer rate constant of Au upon AuNP modification.

Several methodologies for biosensor construction were evaluated involving different AuNP and enzyme ratios and different incubation times for the formation of bioconjugates. The results indicated higher stability over time for the biosensors employing the $AuNP_{MUA}$ and $AuNP_{MBA}$, with more than 90% of the initial sensitivity value being maintained after 1 month of use, alongside higher repeatability and reproducibility values, when compared to the $AuNP_{CIT}$-based biosensor. The higher sensitivity was achieved by the biosensor containing $AuNP_{MBA}$ and SOD in the ratio of 0.3:1 w/v incubated for 1 day, with a detection limit as low as 1 μM. The interference study and the recovery study results obtained in cell culture media support the applicability of the biosensors for the in vivo monitoring of superoxide in cell culture analysis.

**Supplementary Information** The online version contains supplementary material available at https://doi.org/10.1007/s00604-022-05352-z.

**Acknowledgements** The authors thank Dr. George E. Stan for the FT-IR measurements.

**Funding** Financial support from the Executive Agency for Higher Education, Research, Development and Innovation Funding (UEFISCDI), Romania, Project code PN-III-P1-1.1-TE-2019–0387 and PN-III-P1-1.1-PD-2019–0100, and Romanian Ministry of Research and Innovation through Operational Programme Competitiveness 2014–2020, Project NANOBIOSURF-SMIS 103528.

## Declarations

**Competing interests** The authors declare no competing interests.

## References

1. Kucherenko IS, Soldatkin OO, Kucherenko DY, Soldatkina OV, Dzyadevych SV (2019) Advances in nanomaterial application in enzyme-based electrochemical biosensors: a review. Nanoscale Adv 1:4560–4577. https://doi.org/10.1039/C9NA00491B
2. Barsan MM, Brett CMA (2016) Recent advances in layer-by-layer strategies for biosensors incorporating metal nanoparticles. TrAC - Trends Anal Chem 79:286–296. https://doi.org/10.1016/j.trac.2015.11.019
3. Mori S, Kitta Y, Sakamoto H, Takamura E, Suye S. i (2021) Electrochemical characteristics of a gold nanoparticle-modified controlled enzyme–electrode contact junction electrode. Biotechnol Lett 43:1037–1042. https://doi.org/10.1007/S10529-021-03092-3
4. Ramsey AV, Bischoff AJ, Francis MB (2021) Enzyme activated gold nanoparticles for versatile site-selective bioconjugation. J Am Chem Soc 143:7342–7350. https://doi.org/10.1021/JACS.0C11678/ASSET/IMAGES/LARGE/JA0C11678_0005.JPEG
5. Milton RD, Minteer SD (2017) Direct enzymatic bioelectrocatalysis: differentiating between myth and reality. J R Soc Interface 14(131):20170253. https://doi.org/10.1098/RSIF.2017.0253
6. Baslé E, Joubert N, Pucheault M (2010) Protein Chemical Modification on Endogenous Amino Acids. Chem Biol 17:213–227. https://doi.org/10.1016/J.CHEMBIOL.2010.02.008
7. Liu S, Lämmerhofer M (2019) Functionalized gold nanoparticles for sample preparation: a review. Electrophoresis. 40:2438–2461. https://doi.org/10.1002/ELPS.201900111
8. Busch RT, Karim F, Weis J, Sun Y, Zhao C, Vasquez ES (2019) Optimization and structural stability of gold nanoparticle–antibody bioconjugates. ACS Omega 4:15269–15279. https://doi.org/10.1021/ACSOMEGA.9B02276
9. Bartczak D, Kanaras AG (2011) Preparation of peptide-functionalized gold nanoparticles using one pot EDC/Sulfo-NHS coupling. Langmuir 27:10119–10123. https://doi.org/10.1021/LA2022177
10. Jazayeri MH, Amani H, Pourfatollah AA, Pazoki-Toroudi H, Sedighimoghaddam B (2016) Various methods of gold

nanoparticles (GNPs) conjugation to antibodies. Sens Bio-Sensing Res 9:17–22. https://doi.org/10.1016/J.SBSR.2016.04.002
11. Wangoo N, Bhasin KK, Mehta SK, Suri CR (2008) Synthesis and capping of water-dispersed gold nanoparticles by an amino acid: Bioconjugation and binding studies. J Colloid Interface Sci 323:247–254. https://doi.org/10.1016/J.JCIS.2008.04.043
12. Schuetze B, Mayer C, Loza K, Gocyla M, Heggen M, Epple M (2016) Conjugation of thiol-terminated molecules to ultrasmall 2 nm-gold nanoparticles leads to remarkably complex 1 H-NMR spectra. J Mater Chem B 4:2179. https://doi.org/10.1039/c5tb02443a
13. Pillai PP, Huda S, Kowalczyk B, Grzybowski BA (2013) Controlled pH stability and adjustable cellular uptake of mixed-charge nanoparticles. J Am Chem Soc 135:6392–6395. https://doi.org/10.1021/JA4001272
14. Asif M, Liu H, Aziz A, Wang H, Wang Z, Ajmal M, Xiao F, Liu H (2017) Core-shell iron oxide-layered double hydroxide: high electrochemical sensing performance of H2O2 biomarker in live cancer cells with plasma therapeutics. Biosens Bioelectron 97:352–359. https://doi.org/10.1016/J.BIOS.2017.05.057
15. Asif M, Haitao W, Shuang D, Aziz A, Zhang G, Xiao F, Liu H (2017) Metal oxide intercalated layered double hydroxide nanosphere: with enhanced electrocatalyic activity towards H2O2 for biological applications. Sensors Actuators B Chem 239:243–252. https://doi.org/10.1016/J.SNB.2016.08.010
16. Asif M, Aziz A, Ashraf G, Iftikhar T, Sun Y, Xiao F, Liu H (2022) Unveiling microbiologically influenced corrosion engineering to transfigure damages into benefits: a textile sensor for H2O2 detection in clinical cancer tissues. Chem Eng J 427:131398. https://doi.org/10.1016/J.CEJ.2021.131398
17. Sanz CG, Onea M, Aldea A, Barsan MM (2022) Disposable superoxide dismutase biosensors based on gold covered polycaprolactone fibers for the detection of superoxide in cell culture media. Talanta 241:123255. https://doi.org/10.1016/J.TALANTA.2022.123255
18 Duanghathaipornsuk S, Farrell EJ, Alba-Rubio AC, Zelenay P, Kim DS (2021) Detection technologies for reactive oxygen species: fluorescence and electrochemical methods and their applications. Biosensors. 11(2):30. https://doi.org/10.3390/BIOS11020030
19. Di Pasqua AJ, Mishler RE, Ship YL, Dabrowiak JC, Asefa T (2009) Preparation of antibody-conjugated gold nanoparticles. Mater Lett 63:1876–1879. https://doi.org/10.1016/J.MATLET.2009.05.070
20. Chirra HD, Sexton T, Biswal D, Hersh LB, Hilt JZ (2011) Catalase-coupled gold nanoparticles: comparison between the carbodiimide and biotin–streptavidin methods. Acta Biomater 7:2865–2872. https://doi.org/10.1016/J.ACTBIO.2011.01.003
21. Ghosh SK, Pal T (2007) Interparticle coupling effect on the surface plasmon resonance of gold nanoparticles: from theory to applications. Chem Rev 107:4797–4862. https://doi.org/10.1021/CR0680282
22. Kimling J, Maier M, Okenve B, Kotaidis V, Ballot H, Plech A (2006) Turkevich method for gold nanoparticle synthesis revisited. J Phys Chem B 110:15700–15707. https://doi.org/10.1021/JP061667W
23. Li Z, Sheng W, Liu Q, Li S, Shi Y, Zhang Y, Wang S (2018) Development of a gold nanoparticle enhanced enzyme linked immunosorbent assay based on monoclonal antibodies for the detection of fumonisin B1, B2, and B3 in maize. Anal Methods 10:3506–3513. https://doi.org/10.1039/C8AY01036F
24. Marques FC, Oliveira GP, Teixeira RAR, Justo RMS, Neves TBV, Andrade GFS (2018) Characterization of 11-mercaptoundecanoic and 3-mercaptopropionic acids adsorbed on silver by surface-enhanced Raman scattering. Vib Spectrosc 98:139–144. https://doi.org/10.1016/J.VIBSPEC.2018.07.015
25. Michota A, Bukowska J (2003) Surface-enhanced Raman scattering (SERS) of 4-mercaptobenzoic acid on silver and gold substrates. J Raman Spectrosc 34:21–25. https://doi.org/10.1002/JRS.928
26. Ghosh S K, Nath S, Kundu S, Esumi K, Pal T (2004) Solvent and ligand effects on the localized surface plasmon resonance (LSPR) of gold colloids. J Phys Chem B 108:13963–13971. https://doi.org/10.1021/JP047021Q
27. Stevens TE, Pearce CJ, Whitten CN, Grant RP, Monson TC (2017) Self-assembled array of tethered manganese oxide nanoparticles for the next generation of energy storage. Sci Rep 7:39–44. https://doi.org/10.1038/srep44191
28. Yang Y, Huang J, Yang X, Quan K, Wang H, Ying L, Xie N, Ou M, Wang K (2016) Aptazyme–gold nanoparticle sensor for amplified molecular probing in living cells. Anal Chem 88:5981–5987. https://doi.org/10.1021/ACS.ANALCHEM.6B00999
29. Onea M, Bacalum M, Radulescu AL, Raileanu M, Craciun L, Esanu TR, Enache TA (2022) Electrochemical evaluation of proton beam radiation effect on the B16 cell culture. Sci Rep121. 12 (2022) 1–11. https://doi.org/10.1038/s41598-022-06277-6
30. Koposova E, Shumilova G, Ermolenko Y, Kisner A, Offenhäusser A, Mourzina Y (2015) Direct electrochemistry of cyt c and hydrogen peroxide biosensing on oleylamine- and citrate-stabilized gold nanostructures. Sensors Actuators, B Chem 207:1045–1052. https://doi.org/10.1016/j.snb.2014.07.105
31. Zhao R, Liu X, Zhang J, Zhu J, Wong DKY (2015) Enhancing direct electron transfer of glucose oxidase using a gold nanoparticle ltitanate nanotube nanocomposite on a biosensor. Electrochim Acta 163:64–70. https://doi.org/10.1016/j.electacta.2015.02.098
32. Chen X, Li D, Li G, Luo L, Ullah N, Wei Q, Huang F (2015) Facile fabrication of gold nanoparticle on zein ultrafine fibers and their application for catechol biosensor. Appl Surf Sci 328:444–452. https://doi.org/10.1016/j.apsusc.2014.12.070
33. Wang M, Han Y, Liu X, Nie Z, Deng C, Guo M, Yao S (2011) Assembly of layer-by-layer films of superoxide dismutase and gold nanorods: A third generation biosensor for superoxide anion. Sci China Chem 54:1284–1291. https://doi.org/10.1007/s11426-011-4345-4
34. Wu L, Zhang X, Chen J (2014) A new third-generation biosensor for superoxide anion based on dendritic gold nanostructure. J Electroanal Chem 726:112–118. https://doi.org/10.1016/j.jelechem.2014.05.016
35. Saxena U, Chakraborty M, Goswami P (2011) Covalent immobilization of cholesterol oxidase on self-assembled gold nanoparticles for highly sensitive amperometric detection of cholesterol in real samples. Biosens Bioelectron 26:3037–3043. https://doi.org/10.1016/j.bios.2010.12.009
36. Koteshwara Reddy K, Vengatajalabathy Gobi K (2012) Activated direct electron transfer of nanoAu bioconjugates of cytochrome c for electrocatalytic detection of trace levels of superoxide dismutase enzyme. Electrochim Acta 78:109–114. https://doi.org/10.1016/j.electacta.2012.05.159
37. Liu F, Yu R, Wei H, Wu J, He N, Liu X (2022) Construction of a novel electrochemical sensing platform to investigate the effect of temperature on superoxide anions from cells and superoxide dismutase enzyme activity. Anal Chim Acta 1198:339561. https://doi.org/10.1016/j.aca.2022.339561
38. Wu C, Cui M, Chen X, Zhai M, Ren J, Yu C, Yu X, Ji X (2018) Electrochemical determination of the superoxide anion radical using a gold nanoparticle poly(3,4-ethylenedioxythiophene) ferrocyanide multiwalled carbon nanotube glassy carbon electrode. Anal Lett 51:1529–1543. https://doi.org/10.1080/00032719.2017.1381107
39. Wang B, Kang K, Ji X, Liu Y, Li X, Wang N, Ren J (2018) Enhanced electrocatalytic activity of graphene-gold nanoparticles as a superoxide anion biosensor based on immobilized hemin. Int J Electrochem Sci 13:8481–8495. https://doi.org/10.20964/2018.09.12